LANGMUIR

pubs.acs.org/Langmuir Article

Anisotropic Exclusion Effect between Photocatalytic Ag/AgCl Janus Particles and Passive Beads in a Dense Colloidal Matrix

Tao Huang, Sophie Gobeil, Xu Wang, Vyacheslav Misko, Franco Nori, Wim De Malsche, Jürgen Fassbender, Denys Makarov, Gianaurelio Cuniberti, and Larysa Baraban*

Cite This: *Langmuir* 2020, 36, 7091−7099 Read Online

ACCESS | Metrics & More | Article Recommendations | Supporting Information

ABSTRACT: Synthetic nano- and micromotors interact with each other and their surroundings in a complex manner. Here, we report on the anisotropy of active-passive particle interaction in a soft matter system containing an immobile yet photochemical Ag/AgCl-based Janus particle embedded in a dense matrix of passive beads in pure water. The asymmetry in the chemical gradient around the Janus particle, triggered upon visible light illumination, distorts the isotropy of the surrounding electric potential and results in the repulsion of adjacent passive beads to a certain distance away from the Janus particle. This exclusion effect is found to be anisotropic with larger distances to passive beads in front of the Ag/AgCl cap of the Janus particle. We provide insight into this phenomenon by performing the angular analysis of the radii of exclusion and tracking their time evolution at the level of a single bead. Our study provides a novel fundamental insight into the collective behavior of a complex mixture of active and passive particles and is relevant for various application scenarios, e.g., particle transport at micro- and nanoscale and local chemical sensing.

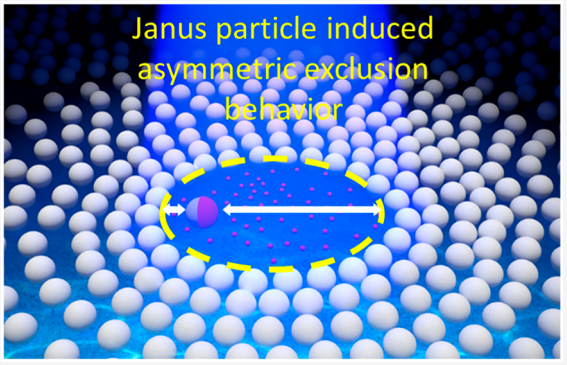

INTRODUCTION

Interactions between species are very common in nature ranging from microorganisms up to mammals. The individual microorganisms within the groups coexist and are driven by a common goal, e.g., to survive or achieve benefits. These groups typically exhibit complex behavioral patterns like schooling or grouping.[1] Characteristic examples include communication of individual cells and microorganisms with each other to form multicellular aggregates when there is a lack of nutrients.[2] Similar to biological systems,[3−5] the study of interactions between synthetic actively moving objects and their environment represents a dynamic research field.[6−9] The interest is primarily motivated by the fact that synthetic nano- and microswimmers that move due to the conversion of chemical energy into mechanical motion[10−18] can mimic numerous functions of natural systems. These artificial model systems have attracted strong attention due to their envisioned impact on life sciences, materials science, and environmental research.[19−22] The key goal is to achieve an efficient control of man-made microswimmers and understand their interactions with the microenvironment to address a broad range of applications, ranging from MEMS and lab-on-a-chip systems through the accomplishment of complex tasks as nanomachinery, nanomedicine, all the way to (bio-) chemical sensing.[23−26]

Recent studies address different systems involving interactions between active particles,[27] active particles and passive beads,[6,28−31] or active particles with a confinement potential, e.g., walls.[32−34] The propulsion of active particles is often achieved by the designed asymmetry of their geometry, e.g., in the case of Janus particles,[35,36] their active side is used to form gradients of temperature,[37] chemical concentration,[6] pressure,[16] or electric potential.[38] Such gradients are typically long-ranged (up to several particle diameters d) and can lead to specific responses of the nearby objects, leading to emerging collective behavior like swarming, schooling,[28,39] exclusion,[40] shape assembling,[41] or those resembling predator−prey interactions in nature.[39]

Rather complex interactions are observed in dense environments of interacting dissimilar species, e.g., when active and passive objects are placed at distances comparable to their linear dimensions. The proximity leads to a strong interaction between passive matrices and local gradients generated by active particles. Similar processes are very common in nature. For instance, "bacterial turbulence"[42] is referred to a large-scale

Special Issue: Advances in Active Materials

Received: January 2, 2020
Revised: January 27, 2020
Published: February 3, 2020

https://dx.doi.org/10.1021/acs.langmuir.0c00012
Langmuir 2020, 36, 7091−7099

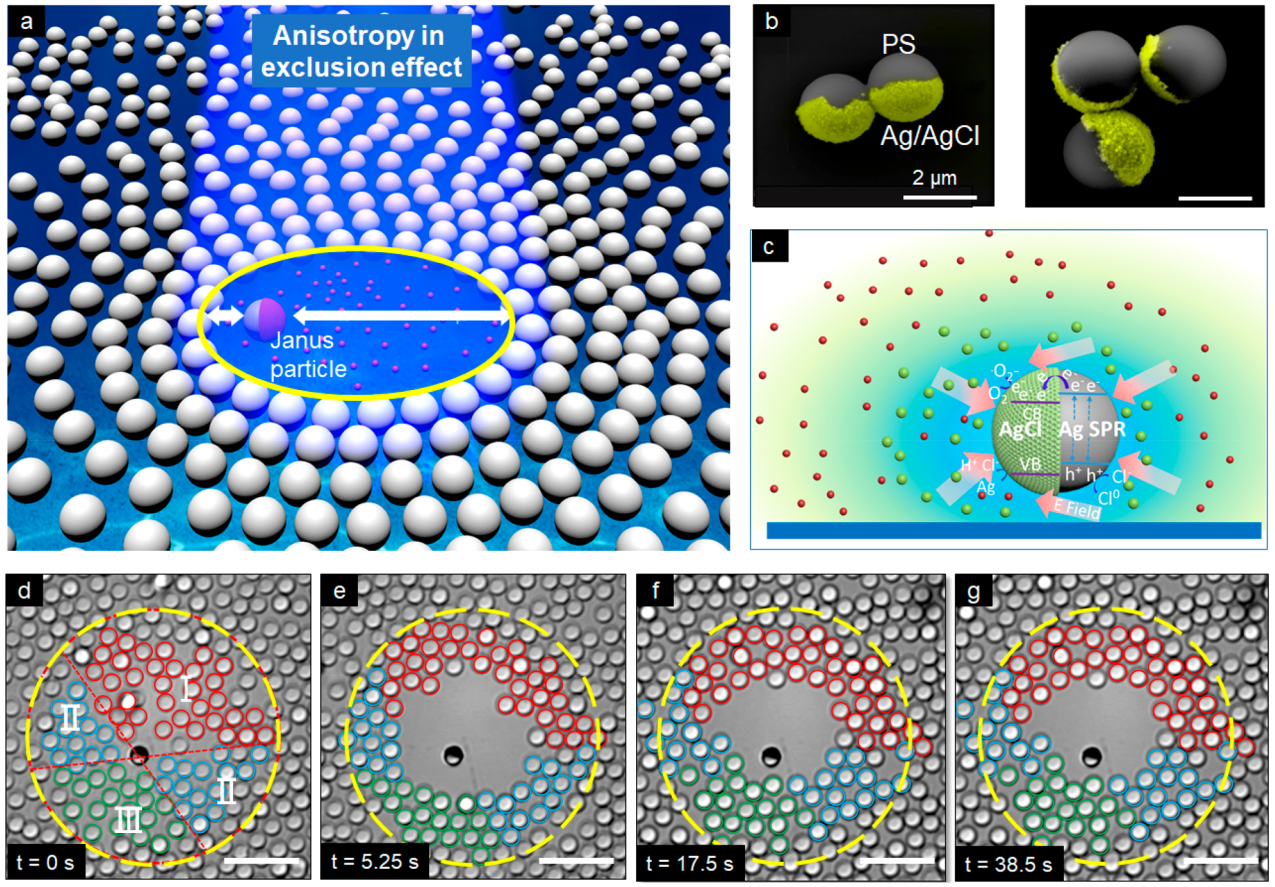

Figure 1. (a) Schematics of the asymmetry in the particle-bead repulsion in a soft-matter system containing an immobilized yet photocatalytically active Janus particle in a dense matrix of passive beads. (b) Scanning electron microscopy (SEM) image of a polystyrene (PS) based Janus particle with its Ag/AgCl cap shown with false color. Scale bar, 2 μm. (c) Schematics of the process when the SPR assisted absorption of visible light by the Ag/AgCl cap of a Janus particle results in a release of ions. Green and red dots depict protons and chlorine ions, respectively. Protons can diffuse faster than chlorine ions, forming a charged area in front of the cap. Pink arrows designate the orientation of the electric field around the Janus particle, oriented inward the cap. (d–g) A sequence of optical microscopy images showing the time evolution of the system of an immobile Janus particle interacting with the surrounding dense passive matrix (SiO_2 beads) under blue light illumination. For the analysis of the distribution of beads, we define three relevant areas indicated in red (in front of the cap of the Janus particle), in green (behind the Janus particle facing its PS side), and in blue (from both sides of the Janus particle). The images are frames of the Video S1. The anisotropy in the particle-bead repulsive interaction leads to anisotropy in the shape of the exclusion area around the Janus particle. Scale bar, 10 μm.

intermittent motion in the form of vortices and can be achieved only at high cell concentration or spermatozoa that tend to form bundles to swim more efficiently in viscous fluids.[43] Therefore, in-depth studies of synthetic interacting systems using statistical approaches[44] help us to not only understand the competing interactions governing the behavior of the system but also explore the impact of active particles on dense environments. In this respect, there has been considerable interest in the collective behavior of dense assemblies of hard sphere-like active or self-propelled particles close to the glass transition,[44−47] as well as the phase behavior of a dense active suspension of self-propelled colloids.[48,49] While dense systems of passive beads and active particles are actively investigated, the *anisotropy in the particle-bead* interactions in a dense matrix, (e.g., amorphous, glassy or crystal[50]) still lacks even a phenomenological description.

Here, we study the anisotropy in the interaction of visible light-driven Ag/AgCl-based spherical Janus particles embedded in a dense matrix of passive SiO_2 beads in pure water (Figure 1a). In contrast to prior works,[35,36] we consider the case when Janus particles are fixed to a glass substrate. Therefore, we primarily track the dynamic properties of the surrounding passive beads. We observe an anisotropic profile of the repulsive interaction between active Janus particles and passive beads and explain it as a result of an asymmetry in the chemical gradient around the Janus particle, triggered upon visible light illumination. This leads to a distortion in the initially isotropic surrounding electric potential and results in the asymmetric exclusion of passive beads around the Ag/AgCl cap. We follow the time evolution of a spatial distribution of passive beads and analyze their displacement around the Janus particle. We describe two limiting cases: when a Janus particle is completely immobile and when it can perform rotational but not translational motion. With this study, we provide new insights into the rotational dynamics of photocatalytically active Janus particles embedded in a dense matrix of passive beads. We anticipate that these phenomena, peculiar for electro-kinetic motors, can only be observed due to the confinement imposed by a dense environment.

■ EXPERIMENTAL SECTION

Photocatalytic Ag/AgCl spherical Janus particles were fabricated as demonstrated elsewhere.[35,36] In brief, monolayers of polystyrene spheres with diameters of 2 μm are deposited with a 60 nm thick layer

https://dx.doi.org/10.1021/acs.langmuir.0c00012
Langmuir 2020, 36, 7091−7099

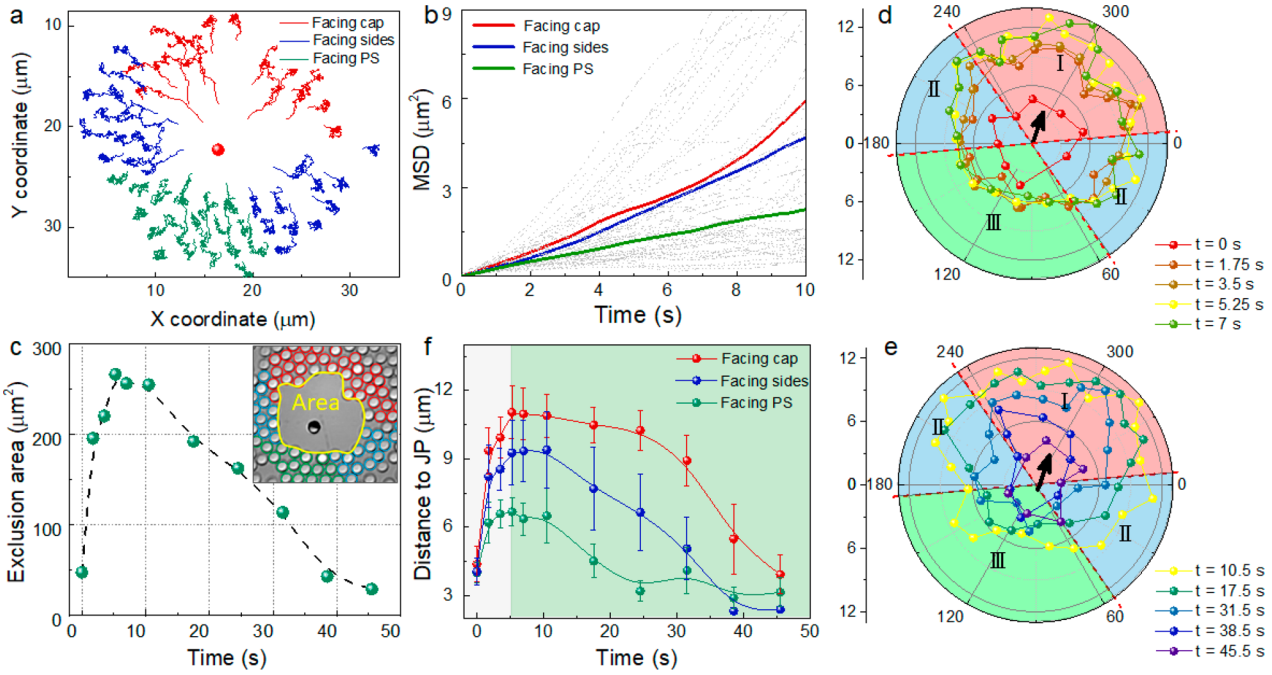

Figure 2. Experimental study of the interaction process in a system containing an immobile Janus particle and passive beads under blue light illumination. (a) Trajectories of passive beads, which are coded accordingly to the color scheme introduced in Figure 1d, i.e., accounting for the initial location of a passive bead with respect to the orientation of the cap of the Janus particle. (b) The corresponding MSD curves for all tracked passive beads (gray lines). The MSD curves shown with red, blue, and green colors are the result of averaging over all MSD curves taken of the beads belonging to one of the three groups. (c) The time evolution of the exclusion area. The insert demonstrates one of the snapshots of the Video S1 (illumination for 5.25 s), with the exclusion area indicated by a yellow line. Scale bar, 4 μm. (d, e) The time evolution of the distance between a Janus particle and the first layer of passive beads. The Janus particle is located in the center of the graph, and the orientation of the main symmetry axis of the cap is indicated with the black arrow. (f) The time evolution of the average distance between a Janus particle and the first layer of passive beads. The averaging is carried out over all passive beads belonging to the indicated region color coded in red, blue, or green in the panels d and e.

of silver, which is converted to a silver chloride by placing capped particles in a $FeCl_3$/PVP solution. Janus particles with the synthesized Ag/AgCl caps (Figure 1b) are washed in deionized (DI) water using a centrifugation process and suspended in DI water for further use.

When such Janus particles are illuminated with blue light (450 nm -470 nm, intensity 137 μW/mm^2), they reveal self-propulsion (Figure S1).[35] This is attributed to the coupling of the plasmonic light absorption by a Ag/AgCl cap[51] and the efficient photochemical production of ions at the cap structure.[52] Namely, as a result of the photochemical reaction, AgCl is reduced to Ag producing protons and chloride ions (Figure 1c). As protons have a significantly higher diffusivity than chlorine ions (D_{H^+} = 9.311 × 10^{-5} cm^2 s^{-1} versus D_{Cl^-} = 1.385 × 10^{-5} cm^2 s^{-1}), a local electric field is generated around the Janus particle.[8,28,36,53] This electric field is oriented inward, i.e., toward the cap (Figure 1c).[8,54,55] The rate of the photochemical reaction is found to be time-dependent. This conclusion is based on the analysis of the motile Janus particles where we observed individual active Janus particles moving with the initial average speed of 20 μm/s, which then gradually decreased to 8 μm/s in the following 20−50 s (Figure S1). A similar behavior with the exponential decay of the velocity with time was observed by Wang's group and is attributed to the self-consumption of AgCl.[54]

To understand how the dynamics of the passive matrix are affected by active particles, we fixed Janus particles on a substrate and then added a suspension of size-matched chemically inert silica beads. Under a reference white light illumination (light intensity of 1.3 μW/mm^2), passive beads display Brownian diffusion. Janus particles and passive beads interact via repulsive electrostatic interaction due to a similar negative ζ potential (ζ_{JP} = −15.1 ± 3.6 mV, ζ_{PP} = −38.7 ± 0.9 mV). Once the blue light illumination is turned on (450 nm -470 nm, intensity 137 μW/mm^2), the photocatalytic decomposition of AgCl at the cap of Janus particles locally releases charged species into the solution. The electric field pointing toward the Ag/AgCl cap acts electrophoretically on the negatively charged silica beads and generates their repulsion from the Janus particles.[35,36,54] We focus on the dynamics of the surrounding passive beads that efficiently reflect the transient processes in the system.

RESULTS AND DISCUSSION

We consider two cases to address the effect of asymmetry in the exclusion behavior: (a) when active particles are fixed to the surface and can perform neither translational nor rotational motion and (b) when only translational motion of the active particle is suppressed and a Janus particle can rotate around its axis.

Active Janus Particles Are Immobile. In this series of experiments, Janus particles are photocatalytically active but they do not perform translational and rotational motions. The density of passive beads in this experiment is 0.151 particles/μm^2 (Figure S2). Once the blue light is on, the repulsion between the Janus particles and passive silica beads is initiated (Figure 1d−g, Video S1). The data clearly demonstrates that the distance from the PS side of the Janus particle to passive beads is smaller than the distance from the Ag/AgCl cap of the Janus particle. To address this asymmetry in the interaction process, we focus on the analysis of several layers of passive beads around the Janus particle (within a circle with a radius of about 12 μm) as those beads are mostly affected by the photochemical reaction. The concentration of the products of the photocatalytic reaction in front and at the sides of the cap of the Janus particle is high. There are no ions generated at the PS side of the Janus particle. Still, diffusional processes form

https://dx.doi.org/10.1021/acs.langmuir.0c00012
Langmuir 2020, 36, 7091−7099

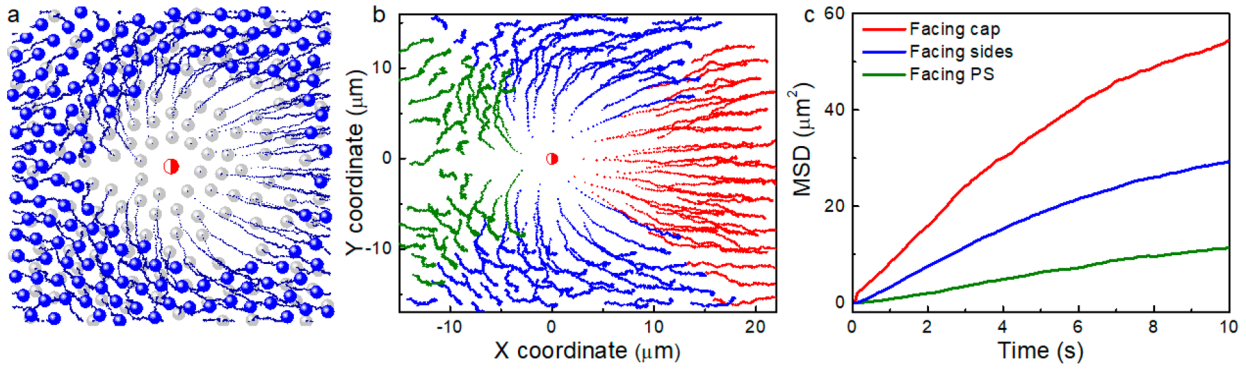

Figure 3. Theoretical study of the interaction process in a system containing an immobile Janus particle and passive beads. (a) Two overlaid snapshots from the simulation data revealing a distribution of passive beads right after blue light is turned on (t = 0.001 s; gray circles) and after illumination for 5 s (blue circles). Trajectories of passive beads are shown by dotted lines. (b) Trajectories of passive beads, which are coded accordingly to the color scheme introduced in Figure 1d, i.e., accounting for the initial location of a passive bead with respect to the orientation of the cap of the Janus particle: in front of the cap of the Janus particle (red dotted lines), on the sides (blue dotted lines), and behind the Janus particle facing its PS side (green dotted lines). (c) MSD curves shown with red, blue, and green colors are the result of averaging over all MSD curves taken of the beads belonging to one of the three groups. Further details are summarized in Figure S4.

"tails of the distribution" and induce less pronounced repulsion between the Janus particle and passive beads. For further quantitative analysis of the temporary evolution of the system, it is insightful to split the dense matrix of passive beads into three different groups according to their locations with respect to the cap of the immobile Janus particle (Figure 1d and Figure S3): in front of the Ag/AgCl cap (red, I), at the particle laterals (blue, II), and in front of the PS side of the Janus particle (green, III). The trajectories of the respective groups of passive beads are shown in Figure 2a. The corresponding mean square displacement (MSD) curves are summarized in Figure 2b. Those passive beads, which are affected by the strongest repulsion (red labeled), acquire the average MSD of about 1.85 μm^2 in 4 s, which is higher compared to the beads at the sides (blue labeled, 1.48 μm^2 in 4 s) and the layers behind the cap (green labeled, 0.93 μm^2 in 4 s).

Due to specificity of the chemical reaction at the surface of the cap, the exclusion effect is time dependent.[54] To quantify this effect, we calculate the time evolution of the exclusion area around the Janus particle, which does not contain passive beads. As shown in Figure 2c, the area rapidly increases to 195 μm^2 after the initial 1.75 s, reaches a maximum of 266 μm^2 at 5.25 s, and then decreases gradually to 29 μm^2 over the next 40 s. To understand this behavior, we analyzed the time-dependent radial distance between the Janus particle (located at the origin point of Figure 2d,e, the orientation of the cap indicated with a black arrow) and the nearest layers of passive beads. In addition, Figure 2d,e provides the angular distribution of the exclusion distance and demonstrates that the strongest repulsion is observed in front of the Ag/AgCl cap, where the concentration of the reaction products is expected to be highest. As shown in Figure 2f, the distance between the cap of the Janus particle and passive beads assigned to the "red" group is 11.0 ± 1.1 μm. At the sides (blue group), the distance is smaller than 9.3 ± 1.4 μm. The smallest distance of 6.7 ± 0.6 μm is found between the Janus particle and those beads which belong to the "green" group facing the PS side of the particle. Similar to the exclusion area, these distances change with time: the distance significantly increases to its maximum value at around 6 s followed by a monotonous decrease during the next 40 s.

The data shows that the onset of the photocatalytic reaction (when the blue light is turned on) initiates the exclusion behavior. With the illumination time, there will be an asymmetry in the spatial profile of the concentration of protons and Cl^- ions around the Janus particle. The highest concentration of the reaction products is in front of the Ag/AgCl cap, leading to the formation of the observed asymmetry in the *radius of exclusion* around the Janus particle. This asymmetry in the interaction process is visible only due to the presence of the confining matrix where the passive beads of the first several layers (closest to the Janus particle) cannot leave the interaction area. After about 6 s, the reaction rate starts to decrease and passive beads tend to move back closer to the location of the Janus particle.

To further explore the asymmetric exclusion process, we performed numerical simulations of the system. While the flow distribution around a Janus particle can be calculated for a simple case of a single Janus particle in free space[56] or near a planar wall,[57−60] the far-flow models are inapplicable for a Janus particle embedded in a dense matrix. When the environment is considered to be homogeneous on a large scale ($\gg d$), simple models of a flow distribution around a Janus particle can be applied. This model is presented in the Experimental Section. We consider an asymmetric flow parameter $\gamma(\theta)$, which is essentially a function of the direction with respect to the axis of the Janus particle. To do so, we assume that the flow strength $\gamma(\theta)$ decreases from the maximum value γ_{max} in front of the cap to the minimum value γ_{min} on the opposite side of the Janus particle (facing its PS side), where $0 \leq \gamma_{min} < \gamma_{max}$. The asymmetric flow strength is modeled by a function $\gamma_{sym} + \gamma_z$, where γ_{sym} is the symmetric part and γ_z is an "anisotropy parameter" ($0 < \gamma_z < \gamma_{max}$) that introduces a shift in the interaction between a Janus particle and a passive bead, along the direction of the cap. Note that the flow of the reaction products around the Janus particle is influenced by the presence of passive beads. However, the model used remains a good approximation even in the case of a dense matrix of surrounding passive beads, due to the following considerations: (1) The experimental setup is three-dimensional and the beads do not block the flow but rather channel it in the gaps between the beads and also above the beads. (2) The impact of this proliferates through the

https://dx.doi.org/10.1021/acs.langmuir.0c00012
Langmuir 2020, 36, 7091−7099

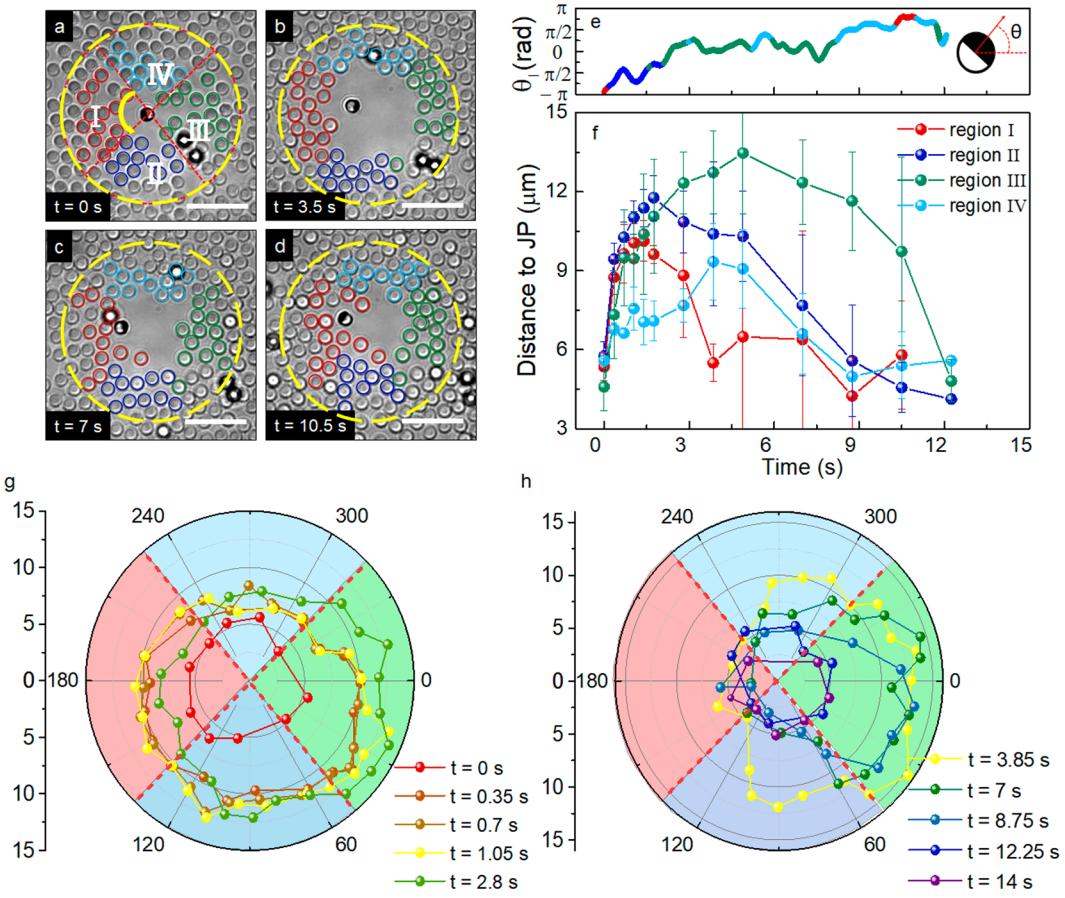

Figure 4. Experimental study of the interaction process in a system containing passive beads and a Janus particle, which can perform rotational but not translational motion, under blue light illumination. (a−d) A sequence of optical microscopy images showing the time evolution of the system. For the analysis of the distribution of beads, we define four relevant areas indicated in red (in front of the cap of the Janus particle), in green (behind the Janus particle facing its PS side), blue (at the left side of the Janus particle), and light blue (at the right side of the Janus particle). The images are frames of the Video S2. Scale bar, 10 μm. (e) The time evolution of the angular orientation of the cap of the Janus particle. The curve is color coded to indicate the orientation of the cap with respect to the location of the initially assigned groups of passive beads. (f, g) The time evolution of the distance between a Janus particle and the first layer of passive beads. The Janus particle is located in the center of the graph and the orientation of the main symmetry axis of the cap is shown in panel (e). (h) The time evolution of the average distance between the Janus particle and the first layer of passive beads. The averaging is carried out over all passive beads belonging to the indicated region color coded in red, green, blue or light blue in the panels f and g.

arrays of the passive beads. This allows us to approximate the flow between the beads as rather "homogeneous", on average (as passive beads are randomly positioned around the Janus particle). (3) The flow decays with the distance from the Janus particle rapidly, which means that the main impact of the flow is exerted on the inner shell of passive beads (as also follows from our measurements and calculations of the MSD). Other passive beads (behind the inner shell) are initially repelled due to the core-to-core interaction with the beads of the inner shell rather than by the flow. After that, when the flow penetrates through the gaps between the beads of the inner shell, other passive beads are carried by this flow.

The simulated time evolution of the distributions of passive beads and their trajectories are shown in Figure 3a for the time interval when the Janus particle is active: From the initial configuration right after the blue light is turned on, at t = 0.001 s (the passive beads are shown by gray circles) to t = 5 s (blue circles), corresponding to the time when the maximum size of the exclusion area is achieved in simulations. The trajectories of the beads are shown by dark blue dotted lines. Similar to the approach to analyze the experimental data (Figure 2), we track separately the simulated trajectories for the beads in front of the Janus particle (red dotted lines in Figure 3b), at the sides (blue dotted lines), and behind the Janus particle (green dotted lines). The averaged MSD curves for beads belonging to each of the three groups are shown in Figure 3c. The detailed analysis of all simulated MSD curves is given in Figure S4. Similar to the experimental data presented in Figure 2b, the MSD analysis indicates a pronounced anisotropy of the exclusion process. The larger MSD values in the simulations as compared to the experiment are explained by the ability of passive beads to freely move while in the experiment they experience a stronger pressure from the dense surrounding matrix.

Active Janus Particle Can Perform Rotational but Not Translational Motion. An even more striking behavior is observed when a photocatalytic active Janus particle can perform rotational fluctuations without translational motion. In this case, depending on the interaction between Janus particles and a substrate, we can expect distinct scenarios, spanning from the diffusive to even subdiffusive rotational motions. The dense passive matrix should be able to "detect" and follow the reorientation of the photocatalytic cap of the Janus particles overtime. In the following, we realize this scenario and study

https://dx.doi.org/10.1021/acs.langmuir.0c00012
Langmuir 2020, 36, 7091−7099

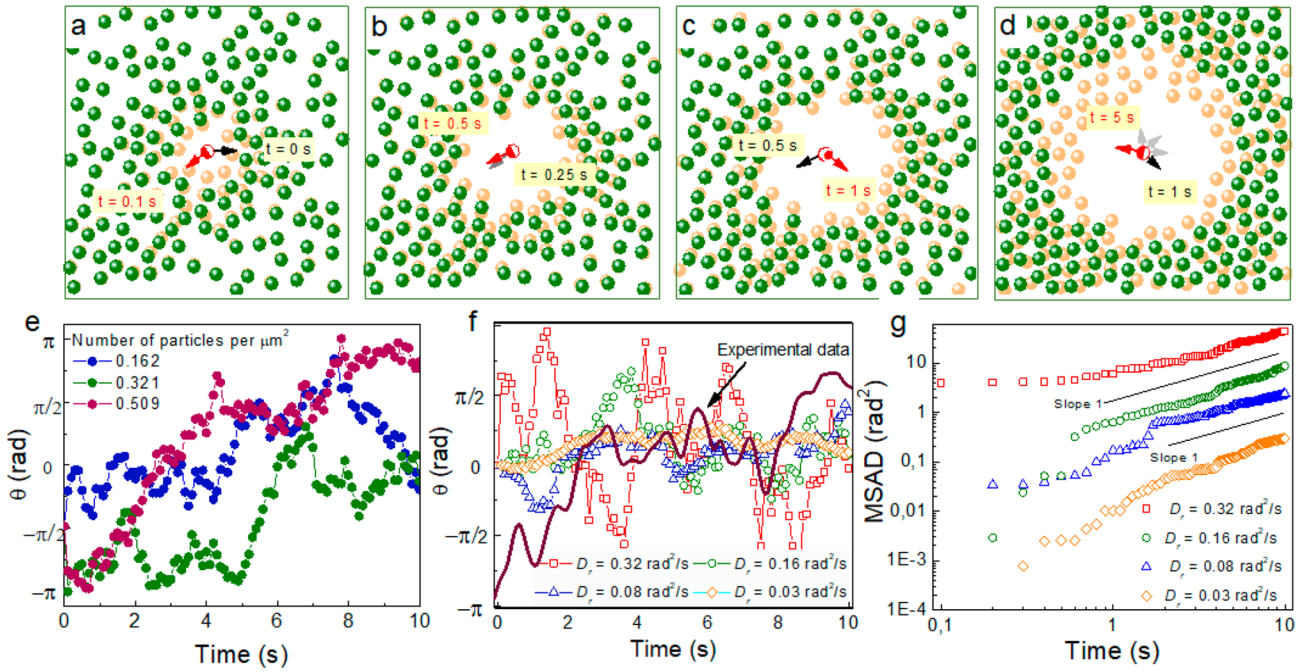

Figure 5. Theoretical study of the interaction process in a system containing passive beads and a Janus particle, which can perform rotational but not translational motion. Panels a–d show time evolution of the interacting system after the blue light is turned on. The snapshots are taken at t = 0.1 s (a), 0.5 s (b), 1 s (c), and 5 s (d) for the density of passive beads, n_{pb}, of 0.509 particles/μm^2. The distribution of passive beads at the previous time step is shown in each panel with orange circles. The Janus particle in the center is shown with a half-filled red circle and its orientation is indicated with a red arrow (gray arrow for the previous time step). (e) The time evolution of the angular orientation of the cap of the Janus particle, $\theta(t)$, for a matrix with different densities of passive beads, n_{pb} = 0.162, 0.321, and 0.509 particles/μm^2. (f) The time evolution of the angular orientation of a Janus particle possessing different rotational diffusion coefficients: D_R = 0.32, 0.16, 0.08, and 0.03 rad^2/s. The brown solid line shows the experimentally measured angular displacement of the Janus particle. (g) The corresponding mean squared angular displacement (MSAD) curves. The straight lines show the slope corresponding to a conventional rotational diffusion.

the trajectories of the rotating Ag/AgCl Janus particles and its interaction with the passive matrix via the analysis of the trajectories and angular distribution of passive colloids in time (Figure 4a–d, Video S2). In this experiment, the density of the passive beads is 0.136 particles/μm^2 (Figure S5). The Janus particle shows a noticeable rotational movement (Figure 4e). Similar to the previous case of an immobile Janus particle, we split the area around the Janus particle into *four regions* (Figure 4a). The regions correspond to the locations of the passive beads with respect to the cap of the Janus particle *at the initial time*. The color coding is as follows: in front of the cap (red, I), at the left side of the particle (blue, II), at the back side of the particle facing its PS side (green, III), and at the right side of the particle (light blue, IV). The trajectories of the Janus particle and passive beads and the corresponding MSD curves are presented in Figure S6a,b, respectively. Due to the asymmetry in the repulsive particle-bead interaction, the rotation of the Janus particle leads to the redistribution of passive beads in time (Figures S7 and S8). The beads, which were assigned to the red group, were the first to respond to the repulsion driven by the photocatalytic reaction. The exclusion area increased significantly during the first 3 s (Figure S6c). We calculated the distance from the Janus particle to the first layer of passive beads (Figure 4f,g; see also Figure S7) and correlated this data to the corresponding angular orientation of the cap of the Janus particle as a function of time (compare Figure 4e,h). In contrast to the data shown in Figure 2f (where the Janus particle is immobile) revealing a monotonous decay of the exclusion distance with time, the distances in Figure 4h display a multipeak behavior, which is in line with the reorientation of the cap over the interaction process. The average distance as a function of time reaches a peak value at 1.4 s and then decreases during 10 s. The peak value is relatively small due to the fact that the cap points toward the red-colored group of particles (region I) for a very short time and is less than 1 s. After this time, the cap starts to rotate toward the blue-colored group of particles (region II). The average distance reaches its maximum of 11.8 μm at 1.75 s. Then the cap oscillates between the locations pointing toward the green group (III) and light blue group (IV). Here, the distances between the Janus particle and passive beads assigned to the green and light blue groups reach a maximum of 13.5 μm at 4.9 s and 9.3 μm at 3.85 s, respectively. During the next 10 s, the cap remains oriented toward the beads of the green group leading to the largest exclusion radius.

To provide a deeper insight in the effect of a dense matrix on the rotational diffusion of a Janus particle, we perform simulations of a system with a rotating Janus particle surrounded by a dense matrix of passive beads. Snapshots revealing the time evolution of the distribution of passive beads from the moment when the blue light is turned on to t = 5 s are summarized in Figure 5a–d. To demonstrate the evolution between the consecutive time steps, we plot the current particle distribution (green circles) and that at the previous time step (gray circles). The angular orientation of the Janus particle is shown for each snapshot by a red arrow for the current time and by a gray arrow for the previous time step. The analysis of the data shown in Figure 5a–d reveals that the shape of the exclusion area changes depending on the angular position of the cap of the Janus particle. In the case when the

https://dx.doi.org/10.1021/acs.langmuir.0c00012
Langmuir 2020, 36, 7091–7099

rotation of the Janus particle is fast enough, we observe a rather isotropic exclusion area (Figure 5d). Still, at each step, the distribution of passive beads is clearly anisotropic. The observed behavior indicates that the reorientation of the Janus particle is associated with an angular redistribution of passive beads following the orientation of the cap of the Janus particle. Therefore, the rotation inside a passive matrix induces a translational motion of passive beads, which should be affected by the density of beads in the matrix. To address this aspect, we simulate the time evolution of the angular orientation of the Janus particle during the exclusion process in the case when the matrix possesses a different density of passive beads, n_{pb} (Figure 5e). While at low densities, the Janus particle executes fast rotations in both directions (the $\theta(t)$ curves for n_{pb} = 0.162 and 0.321 particles/μm^2); these changes become smoother when the density of the matrix is increased (n_{pb} = 0.509 particles/μm^2). In the latter case, sudden changes of the direction of the Janus particle disappear and the angle evolves almost monotonically in one direction. To assess if this behavior is an indication of the crossover to a subdiffusive regime, we perform simulations of the time evolution of the angular orientation of a Janus particle accounting for different rotational diffusion coefficients (Figure 5f): D_R = 0.32, 0.16, 0.08, and 0.03 rad^2/s, simulated for a matrix with the density of passive beads of n_{pb} = 0.509 particles/μm^2. With the brown solid line, we show the experimentally measured angular displacement of the Janus particle. The simulation results are in quantitative agreement with the experiment. The corresponding mean squared angular displacement (MSAD) curves are presented in Figure 5g. Although fast changes of the orientation of the Janus particle become less pronounced with an increase of the density of the surrounding passive matrix, all the simulated MSAD curves show a conventional rotational-diffusion behavior with a slope equal to one. The diffusion regimes are robust, and to observe a crossover to a subdiffusive regime or even the total suppression of the rotational diffusion (or "directional locking"[32]), a Janus particle should be embedded in a very dense, near-crystalline, or glassy matrix.

CONCLUSIONS

To summarize, we quantitatively investigate the repulsive behavior between immobile but photocatalytic Ag/AgCl capped Janus particles embedded in a dense matrix of passive silica beads in pure water. As a result of the photocatalytic reaction, passive beads are repelled away from active Janus particles. The exclusion effect is found to be stronger for these passive beads, which are located in front of the Ag/AgCl cap of the Janus particle. This effect is interpreted in terms of a stronger flow of the products of the chemical reaction from the photocatalytic cap. The profile of the flow is visualized by tracking the trajectories of the passive beads. The study includes the analysis of the MSD of the passive beads as well as the average distances from individual passive beads to the Janus particle. Our conclusion is further supported by the investigation of dynamics in a dense soft matter system containing Janus particles, which can perform rotational but not translational motion. The rotation of the Janus particles results in a redistribution of passive beads according to the angular orientation of the Ag/AgCl cap. We expect that our results will be helpful for a deeper understanding of complex interactions between active and passive particles in various soft matter systems, including those containing synthetic and biological active microswimmers like sperm cells, algae, and bacterial or motor proteins.

ASSOCIATED CONTENT

Supporting Information

The Supporting Information is available free of charge at https://pubs.acs.org/doi/10.1021/acs.langmuir.0c00012.

Data analysis including temporal evolution of the positions of passive beads and Janus particles; analysis of the MSD and calculation of the density of passive beads in the matrix; interactions in a soft matter system containing an immobile Janus particle embedded in a dense matrix of passive SiO_2 beads; interactions in a soft matter system containing a Janus particle, which can perform rotational but not translational motion, embedded in a dense matrix of passive SiO_2 beads (PDF)

Video S1 (AVI)

Video S2 (AVI)

AUTHOR INFORMATION

Corresponding Author

Larysa Baraban − *Helmholtz-Zentrum Dresden-Rossendorf e.V., Institute of Radiopharmaceutical Cancer Research, 01328 Dresden, Germany; Max Bergmann Center of Biomaterials and Institute for Materials Science, Technische Universität Dresden, 01062 Dresden, Germany;* orcid.org/0000-0003-1010-2791; Email: l.baraban@hzdr.de

Authors

Tao Huang − *Max Bergmann Center of Biomaterials and Institute for Materials Science, Technische Universität Dresden, 01062 Dresden, Germany; Helmholtz-Zentrum Dresden-Rossendorf e.V., Institute of Radiopharmaceutical Cancer Research, 01328 Dresden, Germany*

Sophie Gobeil − *Max Bergmann Center of Biomaterials and Institute for Materials Science, Technische Universität Dresden, 01062 Dresden, Germany*

Xu Wang − *Helmholtz-Zentrum Dresden-Rossendorf e.V., Institute of Ion Beam Physics and Materials Research, 01328 Dresden, Germany*

Vyacheslav Misko − *Theoretical Quantum Physics Laboratory, RIKEN Cluster for Pioneering Research, Wako shi, Saitama 351-0198, Japan; μFlow group, Department of Chemical Engineering, Vrije Universiteit Brussel, 1050 Brussels, Belgium*

Franco Nori − *Theoretical Quantum Physics Laboratory, RIKEN Cluster for Pioneering Research, Wako shi, Saitama 351-0198, Japan; Physics Department, University of Michigan, Ann Arbor, Michigan 48109-1040, United States*

Wim De Malsche − *μFlow group, Department of Chemical Engineering, Vrije Universiteit Brussel, 1050 Brussels, Belgium*

Jürgen Fassbender − *Helmholtz-Zentrum Dresden-Rossendorf e.V., Institute of Ion Beam Physics and Materials Research, 01328 Dresden, Germany*

Denys Makarov − *Helmholtz-Zentrum Dresden-Rossendorf e.V., Institute of Ion Beam Physics and Materials Research, 01328 Dresden, Germany;* orcid.org/0000-0002-7177-4308

Gianaurelio Cuniberti − *Max Bergmann Center of Biomaterials and Institute for Materials Science, Technische Universität Dresden, 01062 Dresden, Germany;* orcid.org/0000-0002-6574-7848

Complete contact information is available at:

https://dx.doi.org/10.1021/acs.langmuir.0c00012
Langmuir 2020, 36, 7091−7099

https://pubs.acs.org/10.1021/acs.langmuir.0c00012

Author Contributions

L.B. and T.H. formulated the task. T.H. carried out experimental work with the contribution from S.G., X.W., J.S., and L.B. V.R.M. performed simulations and analyzed the data with contributions from F.N. and W.D.M. The manuscript was written by L.B., D.M., and V.R.M. with contributions from T.H., G.C., J.F., W.D.M., and F.N. All authors have given approval to the final version of the manuscript.

Funding

This work was supported in part by the German Research Foundation (grants BA4986/7−1, BA4986/8−1 and MA5144/14−1). T.H acknowledges the financial support via China Scholarship Council (CSC). V.R.M. and F.N. acknowledge support by the Research Foundation-Flanders (FWO-Vl) and Japan Society for the Promotion of Science (JSPS) (JSPS-FWO Grant No. VS.059.18N). F.N. is supported in part by the MURI Center for Dynamic Magneto-Optics via the Air Force Office of Scientific Research (AFOSR) (Grant No. FA9550−14−1−0040), the Army Research Office (ARO) (Grant No. W911NF-18−1−0358), the Asian Office of Aerospace Research and Development (AOARD) (Grant No. FA2386−18−1−4045), the Japan Science and Technology Agency (JST) (Q-LEAP program and CREST Grant No. JPMJCR1676), the Japan Society for the Promotion of Science (JSPS) (JSPS-RFBR Grant No. 17−52−50023 and JSPS-FWO Grant No. VS.059.18N), the RIKEN-AIST Challenge Research Fund, the FQXi, and the NTT PHi Lab.

Notes

The authors declare no competing financial interest.

■ ACKNOWLEDGMENTS

The authors thank B. Kruppke (TU Dresden) for support with the SEM measurements and B. Ibarlucea (TU Dresden), A. Caspari (Leibniz IPF), L.L. Wang (TU Dresden), and J. Simmchen (TU Dresden) for ζ potential measurements.

■ REFERENCES

(1) Solovev, A. A.; Sanchez, S.; Schmidt, O. G. Collective Behaviour of Self-propelled Catalytic Micromotors. *Nanoscale* **2013**, *5* (4), 1284−1293.
(2) Wingreen, N. S.; Levin, S. A. Cooperation Among Microorganisms. *PLoS Biol.* **2006**, *4* (9), No. e299.
(3) Galajda, P.; Keymer, J.; Chaikin, P.; Austin, R. A Wall of Funnels Concentrates Swimming Bacteria. *J. Bacteriol.* **2007**, *189* (23), 8704−8707.
(4) Angelani, L.; Di Leonardo, R.; Ruocco, G. Self-starting Micromotors in a Bacterial Bath. *Phys. Rev. Lett.* **2009**, *102* (4), No. 048104.
(5) Volpe, G.; Buttinoni, I.; Vogt, D.; Kümmerer, H.-J.; Bechinger, C. Microswimmers in Patterned Environments. *Soft Matter* **2011**, *7* (19), 8810−8815.
(6) Singh, D. P.; Choudhury, U.; Fischer, P.; Mark, A. G. Non-Equilibrium Assembly of Light-Activated Colloidal Mixtures. *Adv. Mater.* **2017**, *29* (32), 1701328.
(7) Hong, Y.; Diaz, M.; Córdova-Figueroa, U. M.; Sen, A. Light-Driven Titanium-Dioxide-Based Reversible Microfireworks and Micromotor/Micropump Systems. *Adv. Funct. Mater.* **2010**, *20* (10), 1568−1576.
(8) Altemose, A.; Sanchez-Farran, M. A.; Duan, W.; Schulz, S.; Borhan, A.; Crespi, V. H.; Sen, A. Chemically Controlled Spatiotemporal Oscillations of Colloidal Assemblies. *Angew. Chem., Int. Ed.* **2017**, *56* (27), 7817−7821.
(9) Wang, L.; Popescu, M. N.; Stavale, F.; Ali, A.; Gemming, T.; Simmchen, J. Cu@ TiO_2 Janus Microswimmers with a Versatile Motion Mechanism. *Soft Matter* **2018**, *14* (34), 6969−6973.
(10) Paxton, W. F.; Kistler, K. C.; Olmeda, C. C.; Sen, A.; St. Angelo, S. K.; Cao, Y.; Mallouk, T. E.; Lammert, P. E.; Crespi, V. H. Catalytic Nanomotors: Autonomous Movement of Striped Nanorods. *J. Am. Chem. Soc.* **2004**, *126* (41), 13424−13431.
(11) Solovev, A. A.; Mei, Y.; Bermúdez Ureña, E.; Huang, G.; Schmidt, O. G. Catalytic Microtubular Jet Engines Self-propelled by Accumulated Gas Bubbles. *Small* **2009**, *5* (14), 1688−1692.
(12) Gao, W.; Pei, A.; Wang, J. Water-driven Micromotors. *ACS Nano* **2012**, *6* (9), 8432−8438.
(13) Zhang, L.; Abbott, J. J.; Dong, L.; Kratochvil, B. E.; Bell, D.; Nelson, B. J. Artificial Bacterial Flagella: Fabrication and Magnetic Control. *Appl. Phys. Lett.* **2009**, *94* (6), No. 064107.
(14) Zhang, L.; Petit, T.; Lu, Y.; Kratochvil, B. E.; Peyer, K. E.; Pei, R.; Lou, J.; Nelson, B. J. Controlled Propulsion and Cargo Transport of Rotating Nickel Nanowires Near a Patterned Solid Surface. *ACS Nano* **2010**, *4* (10), 6228−6234.
(15) Dreyfus, R.; Baudry, J.; Roper, M. L.; Fermigier, M.; Stone, H. A.; Bibette, J. Microscopic Artificial Swimmers. *Nature* **2005**, *437* (7060), 862.
(16) Wang, W.; Castro, L. A.; Hoyos, M.; Mallouk, T. E. Autonomous Motion of Metallic Microrods Propelled by Ultrasound. *ACS Nano* **2012**, *6* (7), 6122−6132.
(17) Abid, J.-P.; Frigoli, M.; Pansu, R.; Szeftel, J.; Zyss, J.; Larpent, C.; Brasselet, S. Light-driven Directed Motion of Azobenzene-coated Polymer Nanoparticles in an Aqueous Medium. *Langmuir* **2011**, *27* (13), 7967−7971.
(18) Soong, R. K.; Bachand, G. D.; Neves, H. P.; Olkhovets, A. G.; Craighead, H. G.; Montemagno, C. D. Powering an Inorganic Nanodevice with a Biomolecular Motor. *Science* **2000**, *290* (5496), 1555−1558.
(19) Guix, M.; Mayorga-Martinez, C. C.; Merkoci, A. Nano/Micromotors in (Bio)chemical Science Applications. *Chem. Rev.* **2014**, *114* (12), 6285−322.
(20) Xu, L.; Mou, F.; Gong, H.; Luo, M.; Guan, J. Light-driven Micro/Nanomotors: from Fundamentals to Applications. *Chem. Soc. Rev.* **2017**, *46* (22), 6905−6926.
(21) Wang, H.; Pumera, M. Fabrication of Micro/Nanoscale Motors. *Chem. Rev.* **2015**, *115* (16), 8704−35.
(22) Safdar, M.; Khan, S. U.; Jänis, J. Progress toward Catalytic Micro-and Nanomotors for Biomedical and Environmental Applications. *Adv. Mater.* **2018**, *30*, 1703660.
(23) Wang, J. Can Man-made Nanomachines Compete with Nature Biomotors? *ACS Nano* **2009**, *3* (1), 4−9.
(24) Ismagilov, R. F.; Schwartz, A.; Bowden, N.; Whitesides, G. M. Autonomous Movement and Self-assembly. *Angew. Chem., Int. Ed.* **2002**, *41* (4), 652−654.
(25) Chałupniak, A.; Morales-Narváez, E.; Merkoçi, A. Micro and Nanomotors in Diagnostics. *Adv. Drug Delivery Rev.* **2015**, *95*, 104−116.
(26) Sánchez, S.; Soler, L.; Katuri, J. Chemically Powered Micro and Nanomotors. *Angew. Chem., Int. Ed.* **2015**, *54* (5), 1414−1444.
(27) Palacci, J.; Sacanna, S.; Steinberg, A. P.; Pine, D. J.; Chaikin, P. M. Living Crystals of Light-activated Colloidal Surfers. *Science* **2013**, *339* (6122), 936−40.
(28) Ibele, M.; Mallouk, T. E.; Sen, A. Schooling Behavior of Light-Powered Autonomous Micromotors in Water. *Angew. Chem., Int. Ed.* **2009**, *48* (18), 3308−3312.
(29) Campbell, A. I.; Ebbens, S. J.; Illien, P.; Golestanian, R. Experimental Observation of Flow Fields Around Active Janus Spheres. *Nat. Commun.* **2019**, *10* (1), 1−8.
(30) Nourhani, A.; Brown, D.; Pletzer, N.; Gibbs, J. G. Engineering Contactless Particle−Particle Interactions in Active Microswimmers. *Adv. Mater.* **2017**, *29* (47), 1703910.
(31) Wang, L.; Käppler, A.; Fischer, D.; Simmchen, J. Photocatalytic TiO_2 Micromotors for Removal of Microplastics and Suspended Matter. *ACS Appl. Mater. Interfaces* **2019**, *11* (36), 32937−32944.

(32) Das, S.; Garg, A.; Campbell, A. I.; Howse, J.; Sen, A.; Velegol, D.; Golestanian, R.; Ebbens, S. J. Boundaries Can Steer Active Janus Spheres. *Nat. Commun.* **2015**, *6*, 8999.
(33) Leeth Holterhoff, A.; Li, M.; Gibbs, J. G. Self-Phoretic Microswimmers Propel at Speeds Dependent upon an Adjacent Surface's Physicochemical Properties. *J. Phys. Chem. Lett.* **2018**, *9*, 5023−5028.
(34) Yu, H.; Kopach, A.; Misko, V. R.; Vasylenko, A. A.; Makarov, D.; Marchesoni, F.; Nori, F.; Baraban, L.; Cuniberti, G. Confined Catalytic Janus Swimmers in a Crowded Channel: Geometry-Driven Rectification Transients and Directional Locking. *Small* **2016**, *12* (42), 5882−5890.
(35) Wang, X.; Baraban, L.; Nguyen, A.; Ge, J.; Misko, V. R.; Tempere, J.; Nori, F.; Formanek, P.; Huang, T.; Cuniberti, G. High-Motility Visible Light-Driven Ag/AgCl Janus Micromotors. *Small* **2018**, *14* (48), 1803613.
(36) Wang, X.; Baraban, L.; Misko, V. R.; Nori, F.; Huang, T.; Cuniberti, G.; Fassbender, J.; Makarov, D. Visible Light Actuated Efficient Exclusion Between Plasmonic Ag/AgCl Micromotors and Passive Beads. *Small* **2018**, *14* (44), 1802537.
(37) Balasubramanian, S.; Kagan, D.; Manesh, K. M.; Calvo-Marzal, P.; Flechsig, G. U.; Wang, J. Thermal Modulation of Nanomotor Movement. *Small* **2009**, *5* (13), 1569−1574.
(38) Paxton, W. F.; Sen, A.; Mallouk, T. E. Motility of Catalytic Nanoparticles Through Self-generated Forces. *Chem. - Eur. J.* **2005**, *11* (22), 6462−6470.
(39) Xu, T.; Soto, F.; Gao, W.; Dong, R.; Garcia-Gradilla, V.; Magaña, E.; Zhang, X.; Wang, J. Reversible Swarming and Separation of Self-propelled Chemically Powered Nanomotors under Acoustic Fields. *J. Am. Chem. Soc.* **2015**, *137* (6), 2163−2166.
(40) Duan, W.; Liu, R.; Sen, A. Transition Between Collective Behaviors of Micromotors in Response to Different Stimuli. *J. Am. Chem. Soc.* **2013**, *135* (4), 1280−1283.
(41) Palacci, J.; Sacanna, S.; Steinberg, A. P.; Pine, D. J.; Chaikin, P. M. Living Crystals of Light-activated Colloidal Surfers. *Science* **2013**, *339*, 1230020.
(42) Wolgemuth, C. W. Collective Swimming and the Dynamics of Bacterial Turbulence. *Biophys. J.* **2008**, *95* (4), 1564−1574.
(43) Lauga, E.; Powers, T. R. The Hydrodynamics of Swimming Microorganisms. *Rep. Prog. Phys.* **2009**, *72* (9), No. 096601.
(44) Berthier, L. Nonequilibrium Glassy Dynamics of Self-propelled Hard Disks. *Phys. Rev. Lett.* **2014**, *112* (22), 220602.
(45) Ni, R.; Stuart, M. A. C.; Dijkstra, M. Pushing the Glass Transition Towards Random Close Packing Using Self-propelled Hard Spheres. *Nat. Commun.* **2013**, *4*, 2704.
(46) Ni, R.; Stuart, M. A. C.; Dijkstra, M.; Bolhuis, P. G. Crystallizing Hard-Sphere Glasses by Doping with Active Particles. *Soft Matter* **2014**, *10* (35), 6609−6613.
(47) Mandal, R.; Bhuyan, P. J.; Rao, M.; Dasgupta, C. Active Fluidization in Dense Glassy Systems. *Soft Matter* **2016**, *12* (29), 6268−6276.
(48) Theurkauff, I.; Cottin-Bizonne, C.; Palacci, J.; Ybert, C.; Bocquet, L. Dynamic Clustering in Active Colloidal Suspensions with Chemical Signaling. *Phys. Rev. Lett.* **2012**, *108* (26), 268303.
(49) van der Meer, B.; Filion, L.; Dijkstra, M. Fabricating Large Two-dimensional Single Colloidal Crystals by Doping with Active Particles. *Soft Matter* **2016**, *12* (14), 3406−3411.
(50) Lozano, C.; Gomez-Solano, J. R.; Bechinger, C. Active Particles Sense Micromechanical Properties of Glasses. *Nat. Mater.* **2019**, *18* (10), 1118−1123.
(51) Simmchen, J.; Baeza, A.; Miguel-Lopez, A.; Stanton, M. M.; Vallet-Regi, M.; Ruiz-Molina, D.; Sánchez, S. Dynamics of Novel Photoactive AgCl Microstars and Their Environmental Applications. *ChemNanoMat* **2017**, *3* (1), 65−71.
(52) Ibele, M.; Mallouk, T. E.; Sen, A. Schooling Behavior of Light-powered Autonomous micromotors in water. *Angew. Chem., Int. Ed.* **2009**, *48* (18), 3308−12.
(53) Yadav, V.; Duan, W.; Butler, P. J.; Sen, A. Anatomy of Nanoscale Propulsion. *Annu. Rev. Biophys.* **2015**, *44*, 77−100.
(54) Zhou, C.; Zhang, H. P.; Tang, J.; Wang, W. Photochemically Powered AgCl Janus Micromotors as a Model System to Understand Ionic Self-Diffusiophoresis. *Langmuir* **2018**, *34* (10), 3289−3295.
(55) Ibele, M. E.; Lammert, P. E.; Crespi, V. H.; Sen, A. Emergent, Collective Oscillations of Self-mobile Particles and Patterned Surfaces Under Redox Conditions. *ACS Nano* **2010**, *4* (8), 4845−51.
(56) Zöttl, A.; Stark, H. Emergent behavior in active colloids. *J. Phys.: Condens. Matter* **2016**, *28*, 253001.
(57) Bayati, P.; Popescu, M. N.; Uspal, W.; Dietrich, S.; Najafi, A. Dynamics near planar walls for various model self-phoretic particles. *Soft Matter* **2019**, *15*, 5644.
(58) Ghosh, P. K.; Misko, V. R.; Marchesoni, F.; Nori, F. Self-propelled Janus Particles in a Ratchet: Numerical Simulations. *Phys. Rev. Lett.* **2013**, *110* (26), 268301.
(59) Takagi, D.; Braunschweig, A. B.; Zhang, J.; Shelley, M. J. Dispersion of Self-propelled Rods Undergoing Fluctuation-driven Flips. *Phys. Rev. Lett.* **2013**, *110* (3), No. 038301.
(60) Yang, W.; Misko, V. R.; Marchesoni, F.; Nori, F. Colloidal Transport Through Trap Arrays Controlled by Active Microswimmers. *J. Phys.: Condens. Matter* **2018**, *30* (26), 264004.

https://dx.doi.org/10.1021/acs.langmuir.0c00012
Langmuir 2020, 36, 7091−7099